A very luminous magnetar-powered Supernova associated with an ultra-long Gamma-ray Burst

Jochen Greiner[1,2], Paolo Mazzali[3,4], D. Alexander Kann[5], Thomas Krühler[6], Elena Pian[7,8], Simon Prentice[3], Felipe Olivares E.[9], Andrea Rossi[7,5], Sylvio Klose[5], Stefan Taubenberger[4,10], Fabian Knust[1], Paulo M.J. Afonso[11], Chris Ashall[3], Jan Bolmer[1,12], Corentin Delvaux[1], Roland Diehl[1], Jonathan Elliott[1], Robert Filgas[13], Johan P.U. Fynbo[14], John F. Graham[1], Ana Nicuesa Guelbenzu[5], Shiho Kobayashi[3], Giorgos Leloudas[15,14], Sandra Savaglio[16,1], Patricia Schady[1], Sebastian Schmidl[5], Tassilo Schweyer[1,12], Vladimir Sudilovsky[17,1], Mohit Tanga[1], Adria C. Updike[18], Hendrik van Eerten[1], Karla Varela[1]

[1] Max Planck Institute for Extraterrestrial Physics, Giessenbachstr. 1, 85748 Garching, Germany

[2] Excellence Cluster Universe, Technische Universität München, Boltzmannstr. 2, 85748, Garching, Germany

[3] Astrophysics Research Institute, Liverpool John Moores University, IC2, Liverpool Science Park, 146 Browlow Hill, Liverpool L3 5RF, United Kingdom

[4] Max Planck Institute for Astrophysics, Karl-Schwarzschild-Str. 1, 85748 Garching, Germany

[5] Thüringer Landessternwarte Tautenburg, Sternwarte 5, 07778 Tautenburg, Germany

[6] European Southern Observatory, Alonso de Córdova 3107, Vitacura, Casilla 19001, Santiago 19, Chile

[7] INAF, Institute of Space Astrophysics and Cosmic Physics, via P. Gobetti 101, 40129 Bologna, Italy

[8] Scuola Normale Superiore, Piazza dei Cavalieri 7, I-56126 Pisa, Italy

[9] Departamento de Ciencias Fisicas, Universidad Andres Bello, Avda. Republica 252, Santiago, Chile

[10] European Southern Observatory, Karl-Schwarzschild-Str. 2, 85748 Garching, Germany

[11] American River College, Physics & Astronomy Dpt., 4700 College Oak Drive, Sacramento, CA 95841, USA

[12] Technische Universität München, Physik Dept., James-Franck-Str., 85748 Garching, Germany

[13] Institute of Experimental and Applied Physics, Czech Technical University in Prague, Horska 3a/22, 128 00 Prague 2, Czech Republic

[14] DARK Cosmology Center, Niels-Bohr-Institut, University of Copenhagen, Juliane Maries Vej 30, 2100 København, Denmark

[15] Department of Particle Physics & Astrophysics, Weizmann Institute of Science, Rehovot 76100, Israel

[16] Universita della Calabria, 87036 Arcavacata di Rende, via P. Bucci, Italy

[17] Astrophysics Data System, Harvard-Smithonian Center for Astrophysics, Garden St. 60, Cambridge, MA 02138, U.S.A.

[18] Roger Williams University, 1 Old Ferry Rd, Bristol, RI 02809, U.S.A.

Abstract

A new class of ultra-long (>10000 s) gamma-ray bursts has recently been suggested [1, 2, 3]. They may originate in the explosion of stars with much larger radii than the normal long GRBs [3] or in the tidal disruptions of a star [3]. No clear supernova had yet been associated with an ultra-long gamma-ray burst. Here we report that a supernova (2011kl) was associated with the ultra-long duration burst 111209A, at $z = 0.677$. This supernova is a factor of >3x more luminous than type Ic supernovae associated with long gamma-ray bursts, and its spectrum is distinctly different. The continuum slope resembles those of super-luminous supernovae, but extends farther down into the rest-frame ultra-violet implying a low metal content. The light curve evolves much more rapidly than super-luminous supernovae. The combination of high luminosity and low metal-line opacity cannot be reconciled with typical type Ic supernovae, but can be reproduced by a model where extra energy is injected by a strongly magnetized neutron star (a magnetar), which has also been proposed as the explanation for the super-luminous supernovae.

GRB 111209A was detected by the *Swift* satellite at 07:12 UT on December 9, 2011. The X-ray and optical counterparts were discovered within minutes of the trigger [12]. The extraordinarily long duration of GRB 111209A was revealed by the continuous coverage with the Konus detector on the WIND spacecraft [13], extending from $\sim 5\,400$ s before to $\sim 10\,000$ s after the *Swift* trigger. The GRB occurred at a redshift of $z = 0.677$ [3], as determined from afterglow spectroscopy. Its integrated equivalent isotropic energy output is $(5.7\pm0.7)\times10^{53}$ erg [13], corresponding to the bright end of the distribution of long-duration GRBs.

The afterglow of GRB 111209A was observed over a period of about 70 days with the 7-channel optical/near-infrared imager GROND [10]. Starting around day 15, the optical light curve of the transient deviates from the earlier afterglow power law decay (Figure 1). The light curve remains essentially flat between day 15 and 30, before it starts to decay again to the host-galaxy level. After subtracting the afterglow and the well-modelled host galaxy emission (Appendix, §1), the excess emission is well-constrained between rest-frame day 6 and 43 after the GRB (Figure 2). It is very similar in shape to other GRB-related supernovae, but reaches a bolometric peak luminosity of $2.8^{+1.2}_{-1.0} \times 10^{43}$ erg/s (corresponding to $\mathrm{M_{bol}} = -20.0$ mag) at 14 rest-frame days, a factor 3 higher than the brightest known GRB-SN (Figure 2).

A VLT/X-shooter spectrum was taken at 11.8 days (rest-frame) after the GRB (Dec. 29, 2011), near the peak of the excess emission [3]. The afterglow and the (minimal) host contribution were subtracted (Appendix, §3) and the resulting spectrum is shown in Figure 3 (blue line). The strong similarity of the evolution in time and color to GRB-associated SNe, together with the spectral shape of the excess emission, leads us to conclude that this emission is caused by the SN associated with GRB 111209A.

Canonical long-duration GRBs are generally accepted to be linked to the core collapse of massive stars stripped of their outer H and He envelopes [5, 6, 7], since every spectroscopically confirmed supernova associated with a GRB has been a broad-lined SN Ic so far. Though the supernova in the ultra-long GRB 111209A also shows no H or He, it is substantially different from classical GRB-SNe. Firstly, it is surprisingly featureless redwards of 300 nm, missing the undulations from spectral line blends typical of broad-lined SNe Ic in association with GRBs [5, 6, 7]. Secondly, the spectrum does not drop in the 300–400 nm (rest-frame) region (Figure 3), suggesting very low metal abundance. Thirdly, applying the standard parametrised SN light curve modelling (Appendix, §4), we derive an ejecta mass of 3 ± 1 $\mathrm{M_\odot}$ and a ^{56}Ni mass of 1 ± 0.1 $\mathrm{M_\odot}$ which implies a very extreme ratio of nickel to ejecta mass. In combination with fourthly, the large luminosity, it is impossible to explain the supernova of GRB 111209A as a canonical stripped-envelope SN (Appendix, §4).

Various models have been suggested to explain the ultra-long duration of GRB 111209A (and a few others), but the otherwise inconspicuous spectral and timing properties of both the prompt and afterglow emission as well as the host properties provided no obvious clues [1, 2, 3, 4, 8, 9, 14]. With the detection of a supernova associated with the ultra-long GRB 111209A, we can immediately discard a tidal disruption event as the origin of GRB 111209A [3]. Also, known supernovae from blue supergiants show hydrogen in their spectra and substantially different light curve properties [15], inconsistent with our observations, and thus ruling out blue supergiants as progenitors [4]. Finally, additional emission from the interaction of the SN ejecta with circum-stellar material is unlikely as well (Appendix, §5).

Our data suggest that in terms of observational properties the supernova of GRB 111209A is intermediate between canonical overluminous GRB-related SNe Ic and the class of super-

luminous supernovae (SLSNe; Figure 3). SLSNe are a sub-class of SNe which are a factor $\sim$100 brighter than normal core-collapse SNe reaching $M_V \lesssim -21$ mag [16, 17]. They show slow rise and late peak times ($\approx$ 15–50 days as compared to typically 9–15 days). Their spectra are characterized by a blue continuum, with a distinctive "W"-shaped spectral feature often interpreted as O II lines [16]. A spinning-down magnetic neutron star is the favoured explanation for the energy input to power the luminous and long-lasting light curves [11]. The comparison of the SN accompanying GRB 111209A with SLSNe is motivated by two observational facts: (1) the spectrum is a blue continuum, extending far into the rest-frame UV, and (2) the peak luminosity is intermediate between GRB-SNe and SLSNe.

We have been able to reproduce the spectrum of the SN using a radiation transport code [18, 19] and a density profile where $\rho \propto r^{-7}$, which is typical of the outer layers of SN explosions. The spectra appear rather featureless but this does not mean that there is no absorption: the UV is significantly depressed relative to a black body. However, it is much less depressed than the spectra of GRB/SNe, indicating a lower metal content. Many metal lines are active in the UV (Fe, Co, Ti, Cr). The smooth appearance of the UV spectrum is the result of the blending of hundreds of lines caused by the large range of wavelengths over which lines are active (line blanketing). Indeed, the photospheric velocity (and density) determines the degree of line blending. We used here photospheric velocities of $v_{ph} \sim 20,000$km/s, and can see increasingly featureless spectra as v_{ph} increases and lines are active at higher velocities (larger blueshift) (Fig. 3). In contrast, SLSNe, which show more line features, have $v_{\mathrm{ph}} \sim 10,000$km/s. In the optical, on the other hand, only few very weak absorptions are visible in our SN spectrum. These are due to Ca II and C II lines. O II lines require large departures from thermal equilibrium because of the very high ionization/excitation potential of their lower levels (20-30 eV). This suggests the presence of X-rays in SLSNe, probably produced by shocks. Our model only has $\sim 0.4\,M_\odot$ of material above the photosphere. The metal content is quite low. It is consistent with 1/4 of the solar metallicity, which could be the metallicity of the star whose explosion caused the GRB and the SN, and there is no evidence of freshly synthesised material mixed-in, unlike in GRB/SNe. This supports the notion that the SN light curve was not powered by ^{56}Ni decay but rather by a magnetar. Fig. 3 shows this model with three different photospheric velocities overplotted on the X-shooter spectrum.

The spectrum can be reproduced without invoking interaction, but the metal abundance is so low that it is unlikely that much ^{56}Ni has been produced. We therefore consider magneto-rotational energy input as the source of luminosity. Depending on the relative strength of magnetar and radioactive decay energy deposition, different peak luminosities as well as rise and decay times can be obtained [20]. One particularly pleasant feature of the magnetar mechanism is that it does not necessarily suffer from strong line blanketing, thus providing a more natural explanation for the observed spectrum.

Using a simple formalism describing rotational energy loss via magnetic dipole radiation and relating the spin-down rate to the effective radiative diffusion time, one can infer the magnetar's initial spin period P_i and magnetic dipole field strength B from the observed luminosity and time to light curve peak t_{peak}. The observed short t_{peak} ($\sim$ 14 rest-frame days) and the moderate peak luminosity require a magnetar with an initial spin period $P_i \sim 12$ ms. Good matches to the light curve can be obtained for a magnetic field strength of $(6-9) \times 10^{14}$ G. Depending on the magnetic field, ejecta mass and kinetic energy have values ranging between 2 and 3 $M_\odot$ and $(2-9) \times 10^{51}$ erg, respectively. Determining the energy and mass is highly uncertain because we do not know how mass is distributed in

velocity space below the photosphere. Still, the ejected mass should be small in order to ensure that the diffusion time is short and the narrow light curve can be matched. The values we find are indeed more typical of normal SNe Ib/c than of GRB/SNe. The values for SN 2006aj, the first SN identified as magnetar-powered [21], are actually not very different. The GRB energy can be reconciled with the maximum energy that can be extracted from a magnetar if the correction for collimation of the GRB jet is a factor of 1/50 or less, which is well within typical values for GRBs [22].

The idea of a magnetar as the inner engine powering GRB-SNe [23, 24], SLSNe [11] or even events like Swift 1644+57 [25], before the general consensus for the latter turned to a relativistic tidal disruption event, is not new. However, in all these cases the magnetar interpretation was one option among several providing a good fit to the data, but never cogent. Also the suggestion that all GRB-SNe are magnetars [24] rather than collapsars, based on the clustering of the kinetic energy of the GRB-SNe at 10^{52} erg, the rotational power of a millisecond neutron star, was only circumstantial evidence.

In contrast, both GRB 111209A and its associated SN are clearly different from GRB/SNe, and at least the SN requires a new explanation. The coincidence suggests that the ultra-long duration of the prompt emission of GRB 111209A and the unusual SN properties are probably related. In the standard fall-back accretion scenario the engine quickly runs out of mass for any reasonable accretion rate and mass reservoir, and is unlikely to be able to power an ultra-long GRB. The collapsar scenario is also excluded on similar grounds. We suggest that both the ultra-long duration of the GRB and the characteristics of the SN are related to the birth and subsequent action of a magnetar, which re-energizes the expanding ejecta and powers an over-luminous supernova. The low metal content seen in the SN spectrum is in accord with the very low host galaxy metallicity (10%-40% solar; Appendix, §4), which is somewhat unusual for such a low-redshift object but commonly seen in SLSN hosts. This particular SN was not quite as luminous as typical SLSNe, and it may represent a population of events that is not easily discovered by SN searches but may have a relatively high rate. This scenario offers a link between GRB/SNe on the one hand, and ultra-long GRBs and SLSNe on the other.

References

[1] Gendre B. et al. The ultra-long gamma-ray burst 111209A: the collapse of a blue supergiant? ApJ **766**, A30 (2013)

[2] Stratta G. et al. The ultra-long gamma-ray burst 111209A: II. Prompt to afterglow and afterglow properties. ApJ **779**, A66 (2013)

[3] Levan A. et al. A new population of ultra-long duration gamma-ray bursts. ApJ **781**, A13 (2014)

[4] Nakauchi D., Kashiyama K., Suwa Y., Nakamura T., Blue supergiant model for ultra-long gamma-ray bursts with superluminous-supernova-like bump. ApJ **778**, A67 (2013)

[5] Galama, T., Vreeswijk, P.M., van Paradijs, J. et al. An unusual supernova in the error box of the gamma-ray burst of 25 April 1998. Nature **395**, 670–672 (1998)

[6] Hjorth, J. et al. A very energetic supernova associated with the gamma-ray burst of 29 March 2003. Nature **423**, 847–850 (2003)

[7] Stanek, K.Z. et al. Spectroscopic discovery of the supernova 2003dh associated with GRB 030329. ApJ **591**, L17–L20 (2003)

[8] Virgili F.J. et al. GRB 091024A and the nature of ultra-long gamma-ray bursts. ApJ **778**, A54 (2013)

[9] Zhang B.-B., Zhang B., Murase K., Connaughton V., Briggs M.S. How long does a burst burst? ApJ **787**, A66 (2014)

[10] Greiner, J. et al. GROND - a 7-channel imager. PASP **120**, 405–424 (2008)

[11] Dessart, L., Hillier, D.J., Waldman, R., Livne, E., Blondin, S. Superluminous supernovae: ^{56}Ni power versus magnetar radiation. MNRAS **426**, L76–L80 (2012)

[12] Hoversten E.A. et al. GRB 111209A: Swift detection of a long burst with an optical counterpart. GCN Circular #12632 (2011)

[13] Golenetskii S. et al. Konus-Wind observation of GRB 111209A. GCN Circular #12663 (2011)

[14] Leloudas, G., et al. Spectroscopy of superluminous supernova host galaxies. A preference of hydrogen-poor events for extreme emission line galaxies. MNRAS (in press; arXiv:1409.8331) (2015)

[15] Kleiser, I.K.W. et al. Peculiar Type II supernovae from blue supergiants. MNRAS **415**, 372–382 (2011)

[16] Quimby, R.M. et al. Hydrogen-poor superluminous stellar explosions. Nature **474**, 487–489 (2011)

[17] Gal-Yam, A. Luminous Supernovae. Science **337**, 927–932 (2012)

[18] Mazzali, P.A., Lucy, L.B. The application of Monte Carlo methods to the synthesis of early-time supernovae spectra A&A **279**, 447–456 (1993)

[19] Mazzali, P. A. Applications of an improved Monte Carlo code to the synthesis of early-time Supernova spectra. A&A **363**, 705–716 (2000)

[20] Kasen, D., Bildsten, L. Supernova light curves powered by young magnetars. ApJ **717**, 245–249 (2010)

[21] Pian, E. et al. An optical supernova associated with the X-ray flash XRF 060218. Nature **442**, 1011–1013 (2006)

[22] Ryan, G., van Eerten, H., MacFadyen, A., Zhang, B.-B. Gamma-Ray Bursts are observed off-axis. ApJ **799**, A3 (2015)

[23] Cano, Z. A trio of gamma-ray burst supernovae: GRB 120729A, GRB 130215A/SN 2013ez, and GRB 130831A/SN 2013fu. A&A **568**, A19 (2014)

[24] Mazzali, P. A. et al. An upper limit to the energy of gamma-ray bursts indicates that GRBs/SNe are powered by magnetars. MNRAS **443**, 67–71 (2014)

[25] Quataert, E., Kasen, D. Swift 1644+57: the longest gamma-ray burst? MNRAS **419**, L1–L5 (2012)

[26] Sauer, D.N. et al. The properties of the 'standard' type Ic supernova 1994I from spectral models. MNRAS **369**, 1939–1948 (2006)

[27] Inserra, C. Super-luminous Type Ic Supernovae: Catching a Magnetar by the Tail ApJ **770**, A128 (2013)

[28] Lunnan, R., et al. PS1-10bzj: a fast, hydrogen-poor superluminous supernova in a metal-poor host galaxy. ApJ **771**, A97 (2013)

[29] Vreeswijk, P.M., et al. The hydrogen-poor superluminous supernova iPTF 13ajg and its host galaxy in absorption and emission. ApJ **797**, A24 (2014)

[30] Yaron, O., Gal-Yam, A. WISeREP - An Interactive Supernova Data Repository. PASP **124**, 668–681 (2012)

[31] Tody, D. IRAF in the nineties. in ASP Conf. **52**, Astronomical Data Analysis Software and Systems II, ed. R.J. Hanisch, R.J.V. Brissenden, & J. Barnes, p. 173 (1993)

[32] Krühler, T. et al. The 2175 Å feature in a gamma-ray burst afterglow at redshift 2.45. ApJ **685**, 376–383 (2008)

[33] Küpcü Yoldaş A. et al. First results of GROND. AIP Conf. Proc. **1000**, 227–231 (2008)

[34] Poole, T. S. et al. Photometric calibration of the Swift ultraviolet/optical telescope. MNRAS **383**, 627–645 (2008)

[35] Schlegel, D., Finkbeiner, D., Davis, M. Maps of dust infrared emission for use in estimation of reddening and cosmic microwave background radiation foregrounds. ApJ **500**, 525–553 (1998)

[36] Vernet J. et al. X-shooter, the new wide band intermediate resolution spectrograph at the ESO Very Large Telescope. A&A **536**, A105 (2011)

[37] Krühler, T. et al. GRB hosts through cosmic time: An emission-line survey of 89 gamma-ray burst selected galaxies between $0.1 < z < 3.6$. A&A (subm.) (2015)

[38] Kann, D.A. et al. Highly luminous supernovae associated with gamma-ray bursts I.: GRB-SN 111209A in the context of other GRB-Supernovae. A&A (to be subm.) (2015)

[39] Arnett, W.D., Type I supernovae. I - Analytic solutions for the early part of the light curve. ApJ **253**, 785–797 (1982)

[40] Valenti, S. et al. The broad-lined Type Ic supernova 2003jd. MNRAS **383**, 1485–1500 (2008)

[41] Mazzali, P. A., et al. The very energetic, broad-lined Type Ic supernova 2010ah (PTF10bzf) in the context of GRB/SNe. MNRAS **432**, 2463–2473 (2013)

[42] Surman, R., McLaughlin, G.C., Hix, W. R., Nucleosynthesis in the Outflow from Gamma-Ray Burst Accretion Disks. ApJ **643**, 1057–1064 (2006)

[43] Perna, R., Duffell P., Cantiello, M., MacFadyen, A.I., The fate of fallback matter around newly born compact objects. ApJ **781**, A119 (2014)

[44] Cardelli, J. A., Clayton, G. C., & Mathis, J. S. The relationship between infrared, optical, and ultraviolet extinction. ApJ **345**, 245–256 (1989)
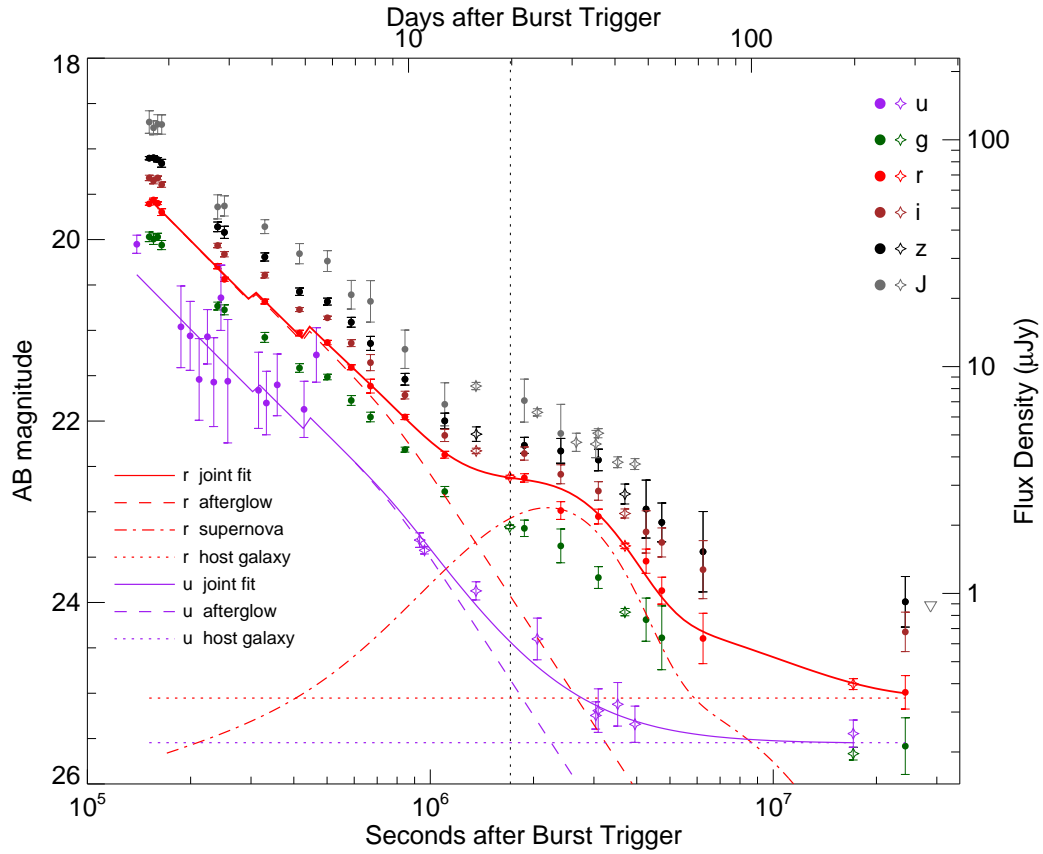
Figure 1: The light curve (GROND data: filled symbols; other data: open symbol) is the sum of the afterglow of GRB 111209A modelled by a broken power law (dashed line), the accompanying supernova 2011kl (thin red line) and the constant GRB/SN host galaxy emission (horizontal dotted line). All measurements (given with 1 uncertainty) are relative to the Swift trigger time and as observed, apart from the Vega-to-AB transformation for the J-band. The solid violet line is the sum of afterglow and host in the u-band, with no sign of the supernova. The solid red line is the sum of afterglow, host and supernova for the r'-band. The vertical dotted line marks the time of the VLT/X-shooter spectrum.
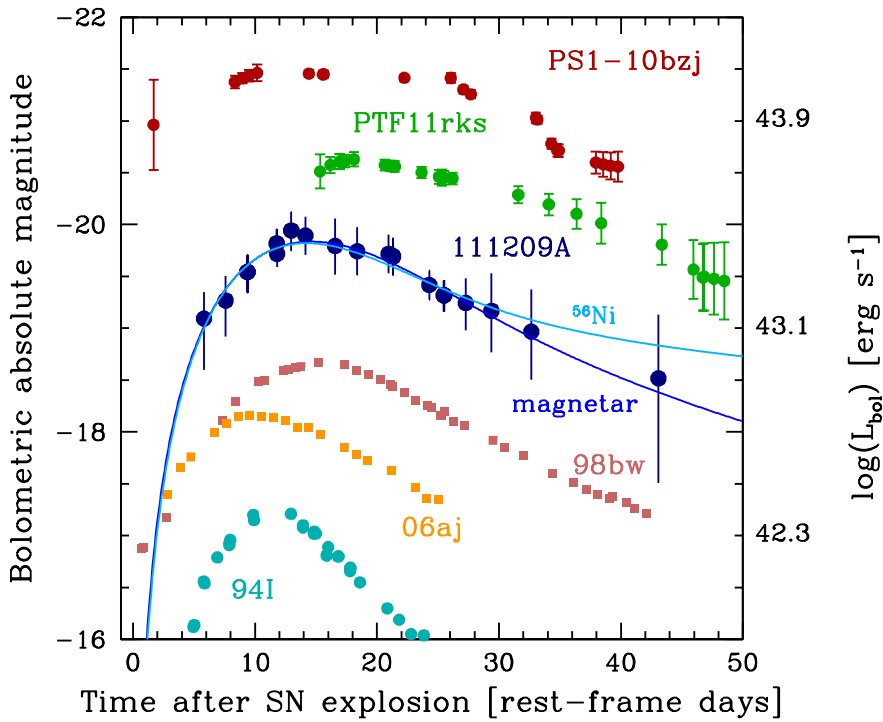
Figure 2: Bolometric light curve of SN 2011kl, corresponding to 230800 nm rest frame (Appendix, 1), compared with those of GRB 980425 / SN 1998bw 5, XRF 060218 / SN 2006aj, the standard type Ic SN 1994I, and the SLSNe PTF11rks and PS1-10bzj (among the fastest-declining SLSNe known so far), all integrated over the same wavelength band with 1 error bars. Solid lines show the best-fitting synthetic light curves computed with a magnetar injection model (dark blue; Appendix, 6) and 56Ni powering (light blue; Appendix, 4), respectively.
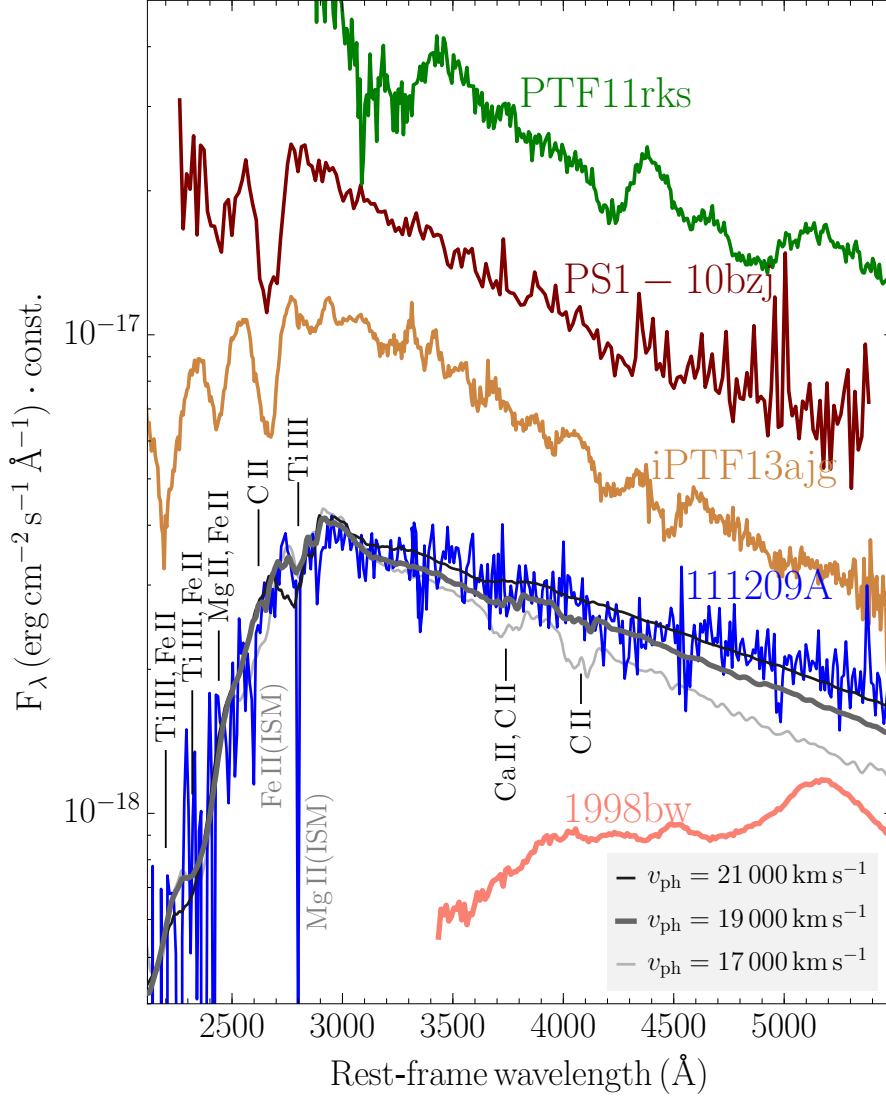
Figure 3: The X-shooter spectrum of SN 2011kl, taken on Dec. 29, 2011 after GRB afterglow and host subtraction and moderate rebinning (Appendix, 1; ED Fig. 2), with its flat shape and high UV flux is distinctly different from the hitherto brightest known GRB-SN 1998bw (red), but reminiscent of some SLSNe (top three curves). The three grey/black lines show synthetic spectra with different photospheric velocities (as labelled), demonstrating the minimum velocity required to broaden unseen absorption around 400 nm rest-frame (CaII, CII), but at the same time explain the sharp cut-off below 280 nm rest-frame. The y-scale is correct for SNe 2011kl and 1998bw; all other spectra are shifted for display purposes.
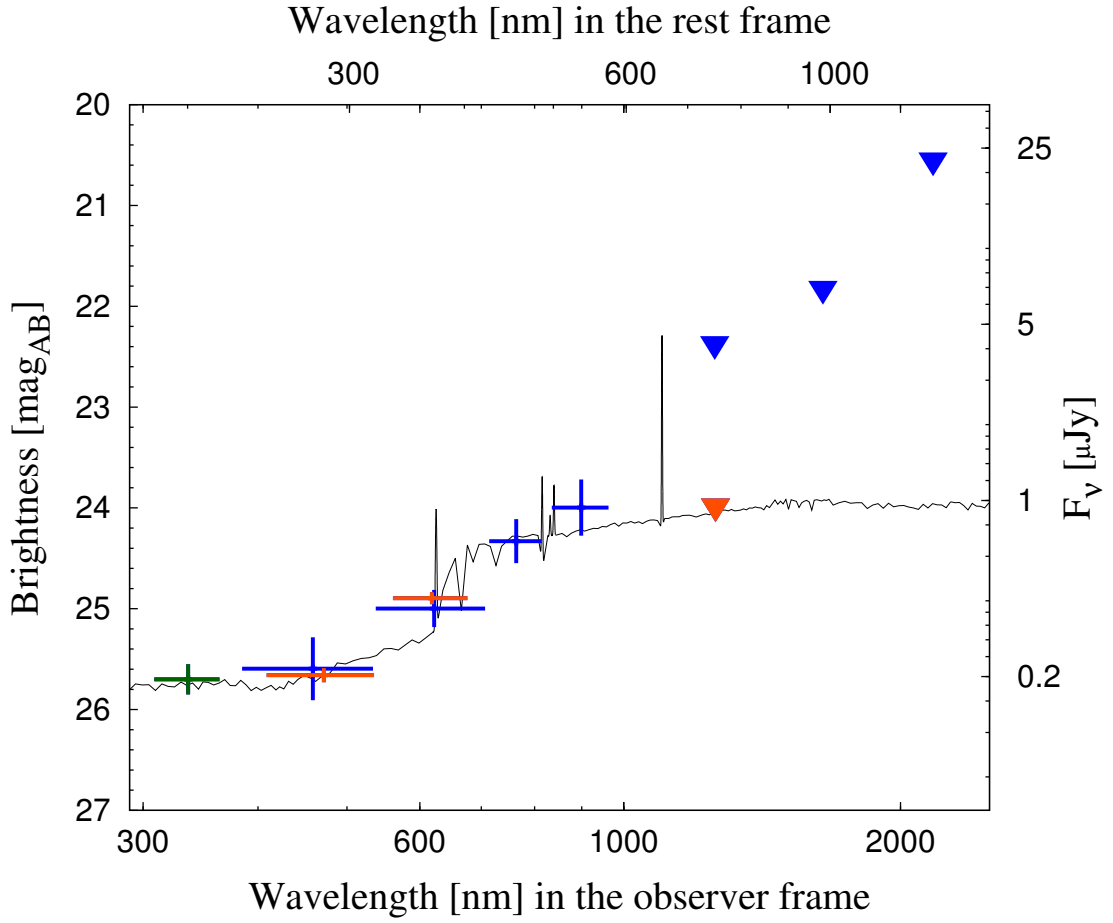
Figure 4: Observed spectral energy distribution of the host galaxy of GRB 111209A. Plotted in blue are GROND $g'r'i'z'$ detections (crosses) and GROND JHK_s upper limits (triangles). Data taken from [3] are $F336W$ (green), Gemini $g'r'$ detections (red crosses) and the J upper limit (red triangle). The best-fit `LePHARE` template of a low-mass, low-extinction, young star-forming galaxy is shown which is very typical for a GRB host.

Table 1: AB Magnitudes of the SN associated with GRB 111209A. The data are corrected for the afterglow and host-galaxy contributions, as well as galactic foreground and rest-frame extinction. The times are in the observer frame. The magnitudes without contemporaneous $g'r'i'z'$-magnitudes are based on data from [3].

Δt [s]	g' mag	r' mag	i' mag	z' mag	J mag
843664	$24.36^{+0.26}_{-0.21}$	$23.92^{+0.23}_{-0.19}$	$24.03^{+0.55}_{-0.38}$	$23.97^{+1.13}_{-0.57}$	$\cdots$
1101930	$24.17^{+0.29}_{-0.24}$	$23.66^{+0.16}_{-0.14}$	$23.80^{+0.44}_{-0.33}$	$23.83^{+0.75}_{-0.48}$	$\cdots$
1358649	$\cdots$	$\cdots$	$\cdots$	$\cdots$	22.38 ± 0.09
1360463	$\cdots$	$\cdots$	$23.28^{+0.12}_{-0.11}$	$\cdots$	$\cdots$
1361742	$\cdots$	$\cdots$	$\cdots$	$23.16^{+0.28}_{-0.25}$	$\cdots$
1705078	23.59 ± 0.04	$\cdots$	$\cdots$	$\cdots$	$\cdots$
1706253	$\cdots$	22.99 ± 0.04	$\cdots$	$\cdots$	$\cdots$
1880549	23.47 ± 0.15	22.90 ± 0.07	22.74 ± 0.13	$22.78^{+0.19}_{-0.18}$	$22.18^{+0.39}_{-0.35}$
2049952	$\cdots$	$\cdots$	$\cdots$	$\cdots$	22.30 ± 0.06
2401323	$23.53^{+0.28}_{-0.27}$	23.25 ± 0.15	22.90 ± 0.17	$22.67^{+0.23}_{-0.22}$	$22.54^{+0.53}_{-0.48}$
2664187	$\cdots$	$\cdots$	$\cdots$	$\cdots$	$22.62^{+0.16}_{-0.15}$
3037306	$\cdots$	$\cdots$	$\cdots$	$\cdots$	$22.58^{+0.22}_{-0.21}$
3085966	$\cdots$	$\cdots$	$\cdots$	$\cdots$	22.41 ± 0.07
3090966	$23.88^{+0.18}_{-0.17}$	23.21 ± 0.11	$23.05^{+0.17}_{-0.16}$	22.70 ± 0.19	$\cdots$
3518554	$\cdots$	$\cdots$	$\cdots$	$\cdots$	22.81 ± 0.09
3692304	$\cdots$	$\cdots$	23.35 ± 0.12	$\cdots$	$\cdots$
3693574	$\cdots$	$\cdots$	$\cdots$	$23.21^{+0.23}_{-0.22}$	$\cdots$
3694905	24.36 ± 0.07	$\cdots$	$\cdots$	$\cdots$	$\cdots$
3696071	$\cdots$	23.60 ± 0.05	$\cdots$	$\cdots$	$\cdots$
3950847	$\cdots$	$\cdots$	$\cdots$	$\cdots$	22.81 ± 0.09
4258444	$24.41^{+0.39}_{-0.37}$	23.80 ± 0.20	$23.63^{+0.42}_{-0.40}$	$23.44^{+0.62}_{-0.58}$	$\cdots$
4732196	$24.69^{+0.63}_{-0.58}$	$24.28^{+0.27}_{-0.26}$	$23.80^{+0.32}_{-0.31}$	$23.67^{+0.48}_{-0.46}$	$\cdots$
6241880	$\cdots$	$25.26^{+0.84}_{-0.74}$	$24.29^{+0.78}_{-0.73}$	$24.27^{+1.57}_{-1.34}$	$\cdots$

Table 2: GROND observations of the afterglow, supernova and host of GRB 111209A. The Δt time gives the mid-time of the observation relative to the *Swift* trigger time, and all magnitudes are in the AB system and not corrected for Galactic foreground extinction. Conversion to Vega magnitudes: $g'_{AB} - g'_{Vega} = -0.062$ mag, $r'_{AB} - r'_{Vega} = 0.178$ mag, $i'_{AB} - i'_{Vega} = 0.410$ mag, $z'_{AB} - z'_{Vega} = 0.543$ mag, $J_{AB} - J_{Vega} = 0.929$ mag, $H_{AB} - H_{Vega} = 1.394$ mag, $K_{S,AB} - K_{S,Vega} = 1.859$ mag. Corrections for Galactic extinction are $A_{g'} = 0.066$ mag, $A_{r'} = 0.046$ mag, $A_{i'} = 0.034$ mag, $A_{z'} = 0.025$ mag, $A_J = 0.015$ mag, $A_H = 0.010$ mag, $A_{K_S} = 0.006$ mag.

Δt [ks]	exp [s]	g' (mag)	r' (mag)	i' (mag)	z' (mag)
151.49	460	20.05 ± 0.05	19.66 ± 0.02	19.36 ± 0.03	19.13 ± 0.02
155.91	460	20.07 ± 0.06	19.62 ± 0.02	19.39 ± 0.03	19.13 ± 0.02
160.33	460	20.05 ± 0.04	19.65 ± 0.02	19.36 ± 0.02	19.15 ± 0.02
164.70	460	20.14 ± 0.05	19.75 ± 0.04	19.43 ± 0.03	19.19 ± 0.04
239.81	919	20.81 ± 0.04	20.35 ± 0.03	20.11 ± 0.02	19.89 ± 0.05
250.95	919	20.85 ± 0.06	20.49 ± 0.02	20.20 ± 0.03	19.95 ± 0.07
329.17	1133	21.16 ± 0.06	20.74 ± 0.03	20.43 ± 0.03	20.22 ± 0.05
415.47	1838	21.49 ± 0.05	21.08 ± 0.03	20.81 ± 0.02	20.60 ± 0.04
501.08	1838	21.59 ± 0.03	21.19 ± 0.02	20.90 ± 0.02	20.71 ± 0.04
588.10	1838	21.85 ± 0.05	21.46 ± 0.03	21.18 ± 0.04	20.94 ± 0.05
669.18	919	22.03 ± 0.05	21.67 ± 0.08	21.40 ± 0.09	21.17 ± 0.08
843.66	1379	22.39 ± 0.03	22.01 ± 0.03	21.75 ± 0.04	21.57 ± 0.06
1101.93	2420	22.86 ± 0.06	22.42 ± 0.04	22.20 ± 0.07	22.03 ± 0.09
1880.55	2952	23.26 ± 0.09	22.68 ± 0.05	22.40 ± 0.07	22.30 ± 0.09
2401.32	4502	23.45 ± 0.19	23.00 ± 0.09	22.63 ± 0.11	22.36 ± 0.14
3090.97	3630	23.80 ± 0.12	23.11 ± 0.08	22.81 ± 0.10	22.46 ± 0.12
4258.44	5384	24.27 ± 0.24	23.60 ± 0.13	23.26 ± 0.23	23.00 ± 0.32
4732.20	5422	24.47 ± 0.35	23.92 ± 0.15	23.38 ± 0.16	23.15 ± 0.21
6241.88	2758	> 24.57	24.45 ± 0.28	23.68 ± 0.32	23.47 ± 0.44
24277.46	3752	25.66 ± 0.31	25.04 ± 0.18	24.36 ± 0.22	24.02 ± 0.28

Δt [ks]	exp [s]	J (mag)	H (mag)	K_s (mag)
151.52	480	18.72 ± 0.12	18.31 ± 0.12	17.84 ± 0.15
155.94	480	18.79 ± 0.08	18.31 ± 0.11	17.87 ± 0.15
160.36	480	18.75 ± 0.10	18.35 ± 0.10	18.01 ± 0.16
164.73	480	18.75 ± 0.11	18.40 ± 0.12	18.09 ± 0.18
239.84	960	19.66 ± 0.13	19.01 ± 0.14	18.71 ± 0.17
250.97	960	19.65 ± 0.11	19.11 ± 0.12	18.98 ± 0.21
329.20	1920	19.87 ± 0.08	19.39 ± 0.12	19.10 ± 0.18
415.49	1920	20.17 ± 0.11	19.88 ± 0.16	19.65 ± 0.26
501.11	1920	20.25 ± 0.11	19.99 ± 0.15	19.94 ± 0.32
588.13	1920	20.62 ± 0.16	20.25 ± 0.19	19.67 ± 0.27
669.20	960	20.70 ± 0.23	20.36 ± 0.29	19.86 ± 0.35
843.69	1440	21.23 ± 0.21	20.71 ± 0.40	20.49 ± 0.46
1101.95	2160	21.83 ± 0.24	20.82 ± 0.25	20.57 ± 0.52
1880.58	2400	21.79 ± 0.24	21.76 ± 0.27	20.70 ± 0.75
2401.32	3600	22.15 ± 0.32	21.86 ± 0.36	> 20.32
3090.99	3240	> 22.25	> 21.85	> 20.22
4258.47	4560	> 21.54	> 21.05	> 19.19
4732.22	4560	> 22.06	> 21.62	> 20.33
6241.91	2880	> 21.52	> 20.91	> 20.06
24277.49	3600	> 22.39	> 21.84	> 20.56

14

Table 3: UVOT observations of the afterglow of GRB 111209A. The Δt time gives the mid-time of the observation relative to the *Swift* trigger time, and all magnitudes are in the AB system and not corrected for Galactic foreground extinction. Conversion to Vega magnitudes: $u_{AB} - u_{Vega} = 1.02$ mag (as given at http://swift.gsfc.nasa.gov/analysis/uvot_digest/zeropts.html). The correction for Galactic extinction, using $E_{(B-V)} = 0.017$ mag [35] and the Galactic extinction curve of [44] is $A_u = 0.085$ mag.

Δt [ks]	exp [s]	u (mag)
139.3566	546	$20.23^{+0.11}_{-0.10}$
187.4401	157	$21.14^{+0.77}_{-0.45}$
199.3795	157	$21.24^{+0.58}_{-0.38}$
211.8172	157	$21.72^{+0.77}_{-0.45}$
223.9091	235.5	$21.25^{+0.42}_{-0.30}$
233.6637	235.5	$21.75^{+0.90}_{-0.49}$
245.1895	156.9	$20.82^{+0.55}_{-0.36}$
256.7393	157	$21.74^{+2.17}_{-0.68}$
286.4793	84.7	> 20.66
315.6230	314.1	$21.84^{+0.70}_{-0.42}$
332.6649	382.4	$21.98^{+0.52}_{-0.35}$
357.8214	844	$21.78^{+0.51}_{-0.34}$
428.4023	578.3	$22.05^{+0.44}_{-0.31}$
465.3887	342	$21.45^{+0.42}_{-0.30}$

Appendix

1. Observations and Data Analysis

Simultaneous imaging in $g'r'i'z'JHK_{\rm s}$ with the 7-channel imager GROND [10] was done on 16 epochs with logarithmic temporal spacing until 72 days after the GRB, when the nearby Sun prevented further observations. A last epoch for host photometry was obtained 280 days after the GRB. GROND data have been reduced in the standard manner using pyraf/IRAF [31, 32, 33]. The optical imaging was calibrated against comparison stars obtained by observing a nearby SDSS field (immediately before the afterglow observation in the third night under photometric conditions) and calibrated against the primary SDSS[1] standard star network. The NIR data were calibrated against the 2MASS catalog. This results in typical absolute accuracies of ± 0.03 mag in $g'r'i'z'$ and ± 0.05 mag in $JHK_{\rm s}$.

We have made use of two other sources of measurements: First, we add u-band observations obtained with *Swift*/UVOT (Tables 3). UVOT photometry was carried out on pipeline-processed sky images downloaded from the *Swift* data centre[2] following the standard UVOT procedure [34], and is fully compatible with earlier, independent publications of the UVOT data [2, 3]. Second, we add selected complementary data, all taken from [3], in particular (i) HST $F336W/F125W$ data from 11.1 and 35.1 days after the GRB, respectively; (ii) two epochs of VLT/FORS2 $g'R_C i'z'$ data during the SN phase, which agree excellently with our data due to [3] using our GROND calibration stars; (iii) a late-time Gemini-S u' observation (198 days after the GRB).

With the constant host galaxy contribution accurately determined at late times in $u'g'r'i'z'J$ (see §3), the afterglow light curve shows clear evidence for a steeper afterglow decay at >10 days post-burst, particularly in

the u' band where there is essentially no contribution from the supernova (as evidenced by the spectrum) and which therefore can be used as a template for the pure afterglow contribution. We link the decay slopes for all filters to be the same. This provides the two decay slopes $\alpha_1 = 1.55 \pm 0.01$ and $\alpha_2 = 2.33 \pm 0.16$, with a break time of $t_{\rm b} = 9.21 \pm 0.47$ days. The u'-band fit is also shown in Fig. 1 to visualize the decomposition. Apart from our much larger data set as provided by the GROND observations, the difference to the decomposition of [3] is the fact that they ignored the host contribution in the redder bands at $\approx 30-50$ days (though they actually note this in their work).

In order to create the SN light curve for each photometric band, we then subtracted both, the afterglow contribution in that band based on the extrapolation of the afterglow light curve, and the host galaxy contribution based on its spectral energy distribution; see §3. The error in the host galaxy subtraction is negligible as the host photometry is accurate to better than 10%, and the host contributes only between 5–15% to the total light during the SN bump. The error on the afterglow subtraction depends on whether or not the decay slope α_2 remained constant after the last secure measurement right before the onset of the SN. The intrinsic GRB afterglow light curves at this late time are observed to only steepen, never flatten. Thus, our afterglow subtraction is conservative, and results in a lower limit for the SN luminosity.

The quasi-bolometric light curve was constructed from GROND $g'r'i'z'J$ photometry and the data from [3] in the following way. First, the individual filter bands have been extinction-corrected with $A_V^{Gal} = 0.06$ mag Galactic foreground [35], and rest-frame $A_V^{host} = 0.12$ mag as derived from the GRB afterglow spectral energy distribution fitting.

---

[1]http://www.sdss.org

[2]www.swift.ac.uk/swift_portal

By deriving quadratic polynomials for sets of three consecutive filters (Simpson's rule) they were then combined to create a quasi-bolometric light curve.

The quadratic polynomials are then integrated over rest-frame wavelength from $3860/(1 + z)$ Å (blue edge of the g' filter) to $13560/(1 + z)$ Å (red edge of the J filter). To transform the integrated flux into luminosity, we employed a distance of $d = 4080$ Mpc, using a concordance cosmology ($\Omega_\Lambda = 0.73$, $\Omega_m = 0.27$, and $H_0 = 71$ km s^{-1} Mpc^{-1}).

The X-shooter [36] spectrum has been reduced with the ESO X-shooter pipeline v2.2.0, in particular for flat-fielding, order tracing, rectification and initial wavelength calibration with an arc lamp. During rectification, a dispersion of 0.4Å/pixel has been used in the UVB/VIS arm, minimizing correlated noise but maintaining sufficient spectral resolution for resolving lines down to $\approx$50 km/s, i.e. a velocity dispersion of 20 km/s. Our own software is used for bad-pixel and cosmic-ray rejection, as well as sky-subtraction and frame shifting and adding [37]. Optimal extraction is applied to the resulting 2D frames, and the one-dimensional spectrum is finally flux calibrated separately for each arm against the GROND photometry. The NIR arm does not contain any useful signal, and thus is not shown in Fig. 3.

The observed spectrum is the sum of light from the GRB afterglow, the GRB host galaxy, and the supernova. After correcting for $A_V^{Gal} = 0.06$ mag [35] Galactic foreground reddening, we corrected for the contribution of the host galaxy using a template fit (§3) on the host photometry (including the J-band measurement of [3]), and subtracted the afterglow based on the extrapolation of the g',r',i',z' GROND light curves to the time of the X-shooter observation. After reducing to the rest-frame, we finally corrected for intrinsic reddening of $E(B - V) = 0.04 \pm 0.01$ mag derived from the GROND afterglow SED

fitting.

2. Association of GRB afterglow, supernova, and host galaxy

We detect narrow absorption lines of Mg II($\lambda2796$, $\lambda2803$), Mg I($\lambda2852$) and Fe II($\lambda2344, \lambda2374, \lambda2382, \lambda2586, \lambda2600$) in the SN spectrum. No change in equivalent widths and redshift is apparent when compared to the afterglow spectrum taken 0.75 days after the GRB [3, 37]. Moreover, these equivalent widths are typical of those seen from host galaxies of bright long-duration GRBs. This relates the SN to the same host galaxy as GRB 111209A.

No offset is measurable in GROND images between GRB afterglow and supernova (δRA <0''.032, $\delta Decl$ <0''.019), which implies that the two events are co-spatial within <200 pc.

3. The host galaxy

During the late-epoch GROND observation the host galaxy is clearly detected in $g'r'i'z'$ in the $3 - 5\sigma$ range (last entry in Table 2). We add HST $F336W$ and Gemini $u'J$ from [3]. Noting that the supernova does not contribute significantly any more during these late epochs (with expected AB magnitudes $g' \approx 28.5$, $r' \approx 28.0$, $i' \approx 27.5$, $z' \approx 27.2$ mag), we employ LePHARE[3] and use the best-fit model (a low-mass, star-forming galaxy) as a template for the host subtraction (see Figure 4). Inferences on the physical properties of the host from this fitting and the absorption/emission line information from the optical/NIR spectra will be published elsewhere [37, 38].

4. Radioactivity cannot power the supernova peak

Modelling the bolometric light curve according to the standard scheme of ^{56}Ni powering [39] and augmented by Co decay [40], an ejecta mass of 3.2±0.5 M$_\odot$ and a ^{56}Ni mass of 1.0±0.1 M$_\odot$ is derived (we used $v_{phot} = $

---

[3]http://www.cfht.hawaii.edu/~arnouts/LEPHARE

20.000 km/s, and a grey opacity of 0.07 ± 0.01 cm^2 g^{-1}, constant in time). The derived ^{56}Ni mass is anomalously large for SNe Ib/c, including GRB/SNe [41]. Such a large ^{56}Ni mass is difficult to reconcile with the very low opacity in the blue part of the spectrum. The continuum flux keeps rising down to 3000 Å without any sign of suppression in the rest-frame UV, implying very low metal line opacity. Also, the ejected mass of $\approx$3 M$_\odot$ as deduced from the light curve width does not resonate with the large ^{56}Ni mass.

While it has been suggested that part of the ^{56}Ni could be synthesised in the accretion disk [42], this is unlikely to proceed at a rate needed in our case. Recent numerical simulations show that for a wide range of progenitor masses (13–40 M$_\odot$), initial surface rotational velocities, metallicities and explosion energies, a disk mass of more than 1 M$_\odot$ (corresponding to $\sim$0.2 M$_\odot$ ^{56}Ni) is difficult to achieve [43], for both cases of compact objects: (i) in the case of heavy fallback, leading to the collapse of the central object into a black hole, the explosion energy is required to be small ($\lesssim$ few $\times$ 10^{48} erg), and more importantly, the disk forms only after a few months due to the large fallback time ($\gtrsim 10^6$ s). (ii) in the case of little fallback, leaving a neutron star behind, only fine-tuned condi-

tions produce fallback disks at all, and these then have lifetimes of at most several hundred seconds.

Thus, a different mechanism must power the SN light curve during the first $\sim$ 40 days (rest frame).

5. Enhanced emission due to interaction with the circumburst medium?

Given the large luminosity, we considered additional emission from the interaction of the supernova ejecta with the circumstellar medium as an alternative possibility. In that case, one may expect narrow Balmer emission lines. While we detect very narrow ($\sigma = 35$ km/s) Hα, Hβ and [OIII] lines in emission, the Balmer fluxes are compatible with the forbidden line flux and with an origin from the global low (0.02 M$_\odot$/yr) star formation rate in this low-metallicity (10%-40% solar) host galaxy [37]. On the other hand, if the progenitor star was heavily stripped, no circumstellar H may be present. Another, more serious constraint is the very blue SN spectrum, which would require a very low density to minimize extinction (though dust may be destroyed by the initial GRB and SN light). This may be at odds with the requirement that the density is high enough to generate the few 10^{43} erg s^{-1} of radiative luminosity observed around the peak.